Magnetic Resonance in Medicine 50:214–219 (2003)

Simple Analytic Variable Density Spiral Design

Dong-hyun Kim,[1,2*] Elfar Adalsteinsson,[1] and Daniel M. Spielman[1]

Variable density spirals have been proposed in a variety of applications, including MR fluoroscopy, cardiac imaging, and MR spectroscopic imaging. In this work, a simple analytic solution for designing a flexible set of variable density spiral trajectory waveforms is presented. The method enables real-time waveform prescription on scanners with limited computational power. Both slew rate-limited and amplitude-limited regimes are incorporated in the design process. Magn Reson Med 50: 214–219, 2003. © 2003 Wiley-Liss, Inc.

Key words: variable density spirals; weighted *k*-space sampling

Most MR images have concentrated energy around the *k*-space origin. Therefore, oversampling near the origin of *k*-space has potential merit for many applications. Variable density spiral *k*-space sampling trajectories achieve this specification while maintaining usefulness for fast imaging applications.

Variable density spirals have been used to increase the temporal resolution of MR fluoroscopy (1), to reduce motion artifacts in cine imaging (2,3), and to reduce the total energy of spatial aliasing artifacts (4). Recently, variable density trajectories have received increased attention due to the interest in multicoil receiver applications. In this case, coil spatial sensitivity profiles can be easily obtained with no increase in the overall scan time (5).

In addition to having the merit of oversampling near the *k*-space origin, a more general analysis of variable density sampling reveals that one can obtain reduced side lobes in the impulse response without a signal-to-noise (SNR) penalty if the applied window function is proportional to the sampling density (6). This property has been applied to MR spectroscopic imaging for reducing ringing artifacts from the subcutaneous lipids (7).

A typical method for designing such trajectories would be to specify the desired sampling density and feed this into a general-purpose gradient waveform design algorithm (8). We present here a simple analytic method for designing variable density spirals, which is an extension to the analytic design algorithm for a conventional spiral trajectory proposed by Glover (9). The method enables real-time prescription on scanners. Simulation and in vivo results illustrating potential applications are given.

THEORY

A general equation of a variable density spiral with sampling density of $\rho(\cdot)$ can be formed as (1):

$$k(\tau) = \lambda \int_0^{\tau} \frac{1}{\rho(\phi)}\, d\phi e^{j\omega\tau} \qquad [1]$$

where $\tau = [0, 1]$ and a function of time, $\omega = 2\pi n$ and n is the number of turns in *k*-space, λ is a constant determined by the desired matrix size and field of view ($\lambda = N/(2 \times FOV)$, N: desired matrix size).

The goal is then to find gradient waveforms, $g(t)$, such that the chosen sampling density, $\rho(\cdot)$, is achieved given the desired resolution and FOV. Slew-rate and amplitude constraints should also be incorporated into the trajectory design such that it is realizable on current gradient hardware. The minimum duration trajectory will normally start in the slew-rate-limited regime and reach the amplitude-limited regime sometime during the readout.

A general class of variable density spiral trajectories with oversampling near the origin can be designed by approximating the intergral term in Eq. [1] by a τ^{α} term, where $\alpha > 1$ depending on the amount of oversampling wanted. The equation can therefore be represented by:

$$k(\tau) = \lambda \tau^{\alpha} e^{j\omega\tau}. \qquad [2]$$

Figure 1 illustrates the various sampling densities achieved for different values of α. As noted by Glover (9), constant density spirals are achieved when $\alpha = 1$, while bigger values of α implies more weighting of low *k*-space values inherent in variable density trajectory. Vice versa, a trajectory with oversampling in high *k*-space values can be achieved with $\alpha < 1$.

Due to the simplicity of Eq. [2], we can derive analytic solutions by differentiating with respect to time. Physically realizable solutions for $\tau(t)$ can then be computed by resampling the trajectory subject to the slew-rate and amplitude constraints as described in Ref. 10.

Amplitude-Limited Case

The amplitude limited case can be obtained by differentiating Eq. [2] with respect to time:

$$g(t) = \frac{\dot{k}(t)}{\gamma} = \frac{\dot{\tau}}{\gamma}\frac{dk}{d\tau} \qquad [3]$$

where γ is the gyromagnetic ratio. Setting the amplitude of $g(t)$ to a maximum available value of g_m and assuming $1 \ll (\omega\tau/\alpha)^2$, the analytic form of $\tau(t)$ is obtained as:

[1]Radiological Sciences Laboratory, Department of Radiology, Stanford University, Stanford, California.

[2]Department of Electrical Engineering, Stanford University, Stanford, California.

Grant sponsors: GE Medical Systems; NIH; Grant numbers: CA 48269; RR09784; AG18942.

*Correspondence to: Dong-hyun Kim, Lucas MRS Imaging Center, Stanford, CA 94305-5488. E-mail: dhkim@stanford.edu

Received 30 October 2002; revised 25 February 2003; accepted 6 March 2003.

DOI 10.1002/mrm.10493
Published online in Wiley InterScience (www.interscience.wiley.com).

$$\tau(t) = \left[\frac{\gamma g_m}{\lambda\omega}(\alpha+1)t\right]^{(1/\alpha+1)}. \quad [4]$$

The trajectory ends when $\tau(t) = 1$. This time ($t = T_{ea}$) can be found from Eq. [4]:

$$T_{ea} = \left[\frac{\gamma g_m}{\lambda\omega}(\alpha+1)\right]^{-1}. \quad [5]$$

Slew-Rate-Limited Case

Likewise, a slew-rate limited form can also be achieved by differentiating $g(t)$ in Eq. [3] with respect to time:

$$s(t) = \dot{g}(t) = \frac{\dot{\tau}^2}{\gamma}\frac{d^2k}{d\tau^2} + \frac{\ddot{\tau}}{\gamma}\frac{dk}{d\tau}. \quad [6]$$

Setting $s(t)$ to a maximum available slew-rate value of s_m and neglecting the second term in Eq. [6], an analytic form of $\tau(t)$ for a slew-rate limited case can be found by:

$$\tau(t) = \left[\sqrt{\frac{s_m\gamma}{\lambda\omega^2}}\left(\frac{\alpha}{2}+1\right)t\right]^{[1/(\alpha/2+1)]}. \quad [7]$$

The ending time ($t = T_{es}$) of this trajectory can also be found by letting $\tau(t) = 1$:

$$T_{es} = \left[\left(\frac{\alpha}{2}+1\right)\sqrt{\frac{s_m\gamma}{\lambda\omega^2}}\right]^{-1}. \quad [8]$$

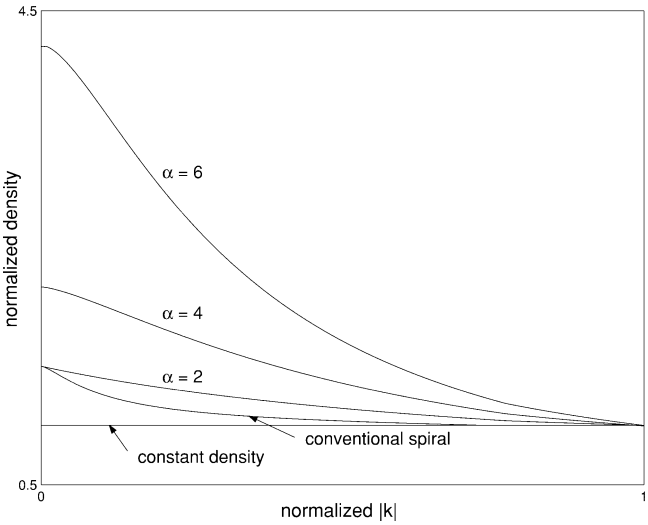

FIG. 1. *k*-Space sampling densities for various values of α as a function of *k*-space radius. Depending on the desired oversampling in the central *k*-space region, different values of α can be used. The density was normalized so that it satisfies the Nyquist sampling at the edge (density = 1) and *k*-space origin density was defined as the number of points within radius of the grid interval. Note, conventional "constant density" spiral design have some degree of oversampling at the origin due to finite gradient slew-rate.

Slew-Rate and Amplitude Limited Case

The above two cases can be combined to satisfy both the slew-rate and amplitude constraints. A typical trajectory designed for minimum readout duration will start off in the slew-rate limited regime and after it has reached its maximum gradient amplitude, it will switch to the amplitude limited regime. The time that this transition occurs ($t = T_{s2a}$) can be found by setting $g(t) = g_m$ in the slew-rate limited regime. Therefore, using $\tau(t)$ of Eq. [7] and solving for $g(t)$:

$$T_{s2a} = \left[\frac{g_m\gamma}{\lambda\omega\dfrac{1}{\dfrac{\alpha}{2}+1}\left(\left(\dfrac{\alpha}{2}+1\right)\sqrt{\dfrac{s_m\gamma}{\lambda\omega^2}}\right)^{[(\alpha+1)/(\alpha/2+1)]}}\right]^{(\alpha+2)/\alpha}. \quad [9]$$

From this time on, the gradients switch to an amplitude-limited trajectory. Note that since the trajectory is discrete in time, T_{s2a} should be rounded to the maximum integer multiple of the sampling interval of the gradients.

An analytic form of n can also be found by noting the distance in k-space when $\tau = 1$ and $\tau = (n-1)/n$ needed to satisfy the Nyquist sampling distance between adjacent trajectory turns. Therefore, the field of view constraint has to satisfy $k(1) - k((n-1)/n) = 1/FOV$, hence the solution for n using Eq. [2] becomes:

$$n = \left[1 - \left(1 - \frac{2}{N}\right)^{(1/\alpha)}\right]^{-1}. \quad [10]$$

The value of α determines the amount of oversampling in the central k-space region (Fig. 1). Generally, bigger α results in more dense sampling of low spatial frequencies. The appropriate value will depend on the application being intended for.

Summary

A simple analytic variable density spiral can be designed by:

$$\tau(t) = \begin{cases} \left[\sqrt{\dfrac{s_m\gamma}{\lambda\omega^2}}\left(\dfrac{\alpha}{2}+1\right)t\right]^{[1/(\alpha/2+1)]} & 0 \le t \le \min(T_{s2a}, T_{es}), \\ \left[\dfrac{\gamma g_m}{\lambda\omega}(\alpha+1)t\right]^{1/(\alpha+1)} & T_{s2a} \le t \le T_{ea} \end{cases} \quad [11]$$

The gradient waveforms $g(t) = g_x(t) + jg_y(t)$ can be found by:

$$g(t) = \frac{\dot{k}(t)}{\gamma} = \frac{\lambda}{\gamma}\frac{\tau(t)^\alpha e^{j\omega\tau(t)} - \tau(t-\Delta t)^\alpha e^{j\omega\tau(t-\Delta t)}}{\Delta t} \quad [12]$$

where Δt is the sampling interval of the gradients. Note that depending on the parameters given, the trajectory can end before reaching the amplitude limited regime (when $T_{s2a} > T_{es}$). But normally, trajectories begin limited by

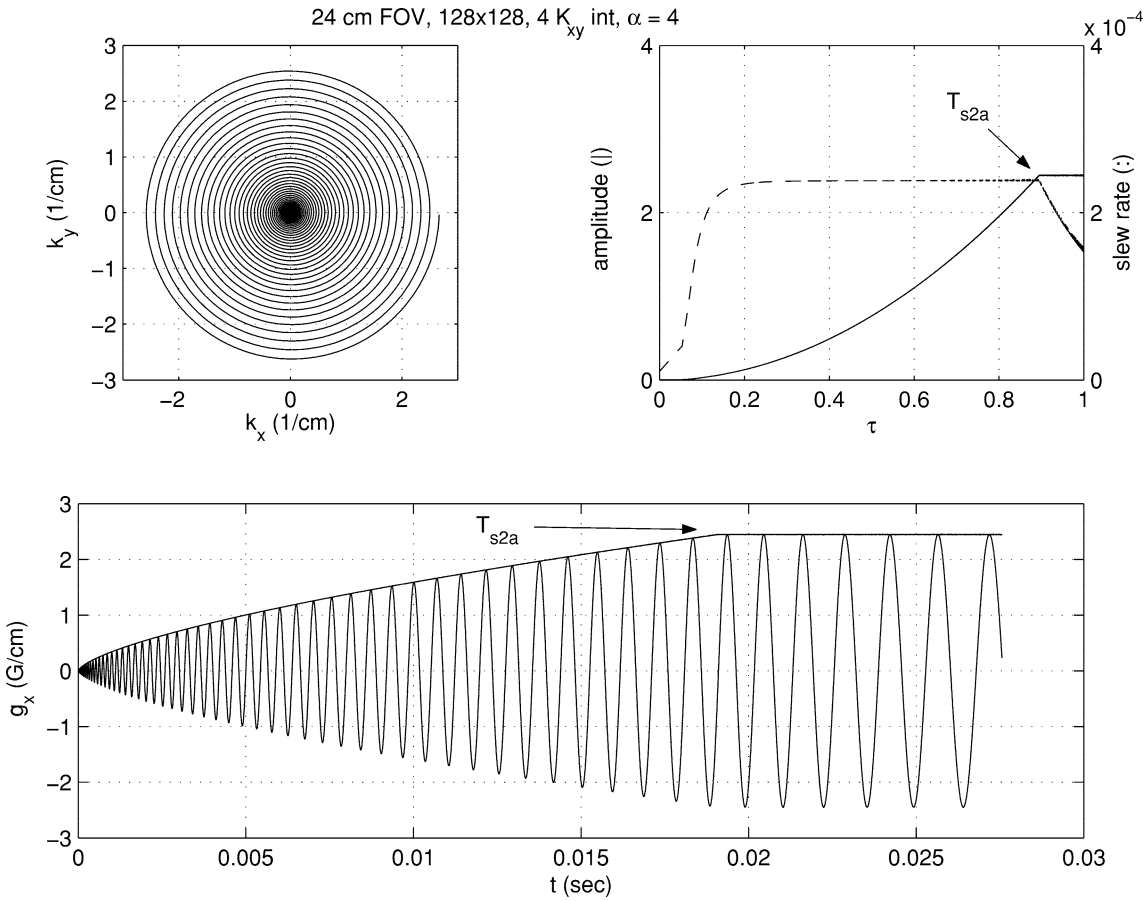

FIG. 2. Design example of a four interleave, 128 × 128 resolution, 24 cm FOV variable density spiral trajectory using gradient characteristics of amplitude: 2.2 G/cm, slew rate: 25 G/cm/ms. Corresponding *k*-space trajectory, amplitude, and slew-rates and gradient values are given.

the slew-rate constraints and at time T_{s2a} convert to the amplitude limited regime. Figure 2 shows a sample waveform design that includes both the slew-rate limited and the amplitude limited cases for a four interleave *k*-space trajectory (N = 128, FOV = 24 cm, and α = 4).

EXPERIMENT AND RESULTS

Variable density spirals, designed using Eq. [12], were implemented into a gradient echo pulse sequence on a GE Signa 1.5 T scanner. A conventional spiral sequence was also used for comparison (9). Two potential applications using the trajectories were investigated.

First, to show usage in MR spectroscopic imaging applications where ringing artifacts due to side lobes are problematic, simulations were performed to illustrate the reduced side lobes using the variable density spirals. Data were reconstructed assuming an impulsive object at the origin (i.e., point spread function) and compared with the conventional spiral acquisition. As pointed out in (7), to keep the SNR and nominal resolution (full width at half maximum, FWHM) the same for the two cases, a 128 × 128 acquisition was assumed for the conventional spirals whereas a 256 × 256 acquisition covering twice the *k*-space was assumed for the variable density spirals (α = 4). Data were apodized according to their density function prior to reconstruction. Figure 3 shows the slice profiles of the reconstructed images from the two acquisitions. As can be seen, variable density spirals show significantly decreased side lobes while maintaining the same nominal resolution.

We also collected experimental data using conventional and variable density spirals with a spectroscopic imaging sequence (11). Two small phantoms filled with water were used for data acquisition. The water images were reconstructed and displayed. For the constant density acquisition, the parameters used were: eight spatial interleaves, one spectral interleave, 32 × 32 matrix size reconstructed onto a 64 × 64 matrix, and 720 Hz spectral bandwidth. The minimum scan time is thus 8 × TR. For the variable density acquisition, the parameters used were: twelve spatial interleaves, three spectral interleaves, 64 × 64 matrix size reconstructed onto a 64 × 64 matrix, and 730 Hz spectral bandwidth. The minimum scan time is thus 12 × 3 × TR. Both acquisitions had the same imaging time by controlling the number of averages acquired. Figure 4 shows the water images obtained from the experiment and the logarithmic magnitude plot through the center slice of both images. Both images were adjusted to be in the same scale. As can be seen in the images, variable density acquisition results in a reduced ringing artifact,

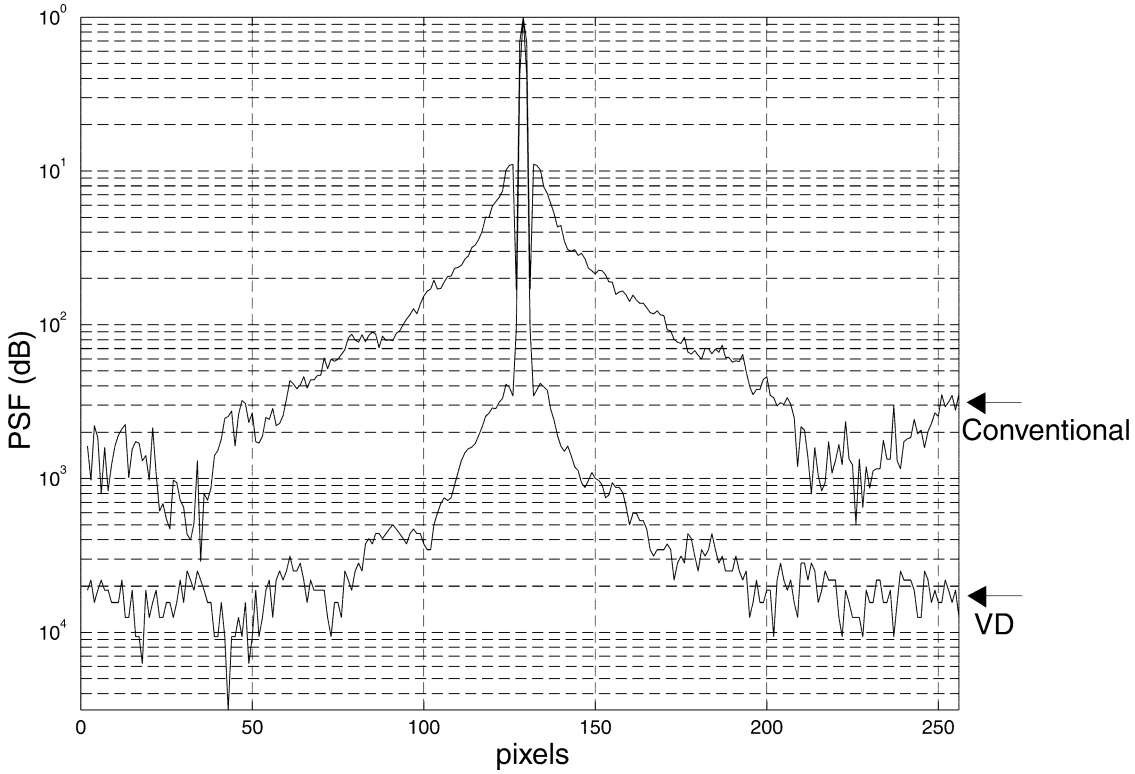

FIG. 3. Cross sectional plot of the simulated point-spread function for variable density (VD) and conventional spiral designs. A simulation of the point-spread function. The middle slice profile is given for the reconstructed impulse function. Side lobes are reduced for variable density (solid) acquisition compared to conventional spirals (dashed) while nominal resolution and SNR are the same.

while reduced sidelobes can be seen in the magnitude plot.

Second, to illustrate the potential application in MR fluoroscopy, in vivo images were obtained using variable density and conventional spiral trajectories designed for a 128 × 128 matrix, 20 cm FOV multislice acquisition (α = 4). To keep the readout length the same for the two trajectories, 16 spatial interleaves were used for the conventional spiral acquisition, whereas variable density spirals were obtained with 24 spatial interleaves. All data reconstructions were performed using gridding with first-order shim correction (12). Figure 5 shows representative slices from the in vivo images obtained using these trajectories. Both images have comparable quality. In a fluoroscopic study, dynamic information would be obtained by continuously acquiring images. In this mode, variable and conventional spiral acquisition can best be compared by computing the temporal updating rate as a function of spatial frequency. Figure 5c plots the temporal updating rate, which is defined as the time it takes for a certain spatial

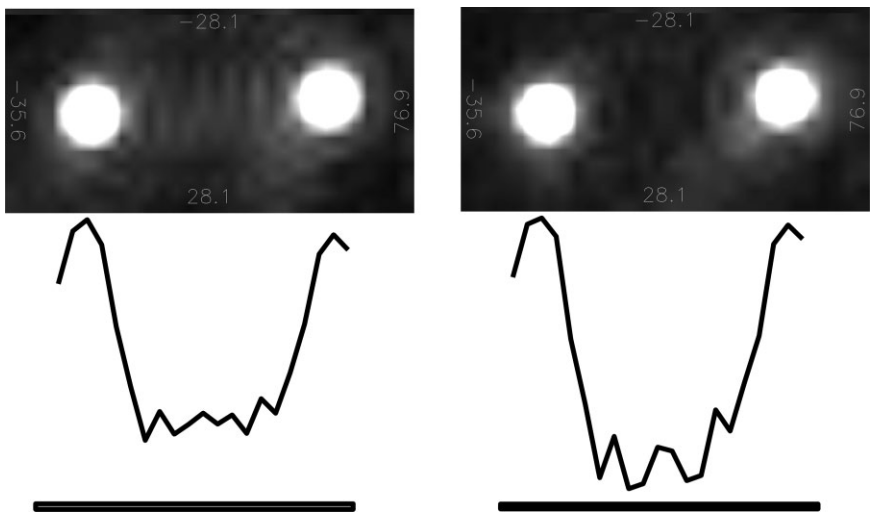

FIG. 4. Reconstructed water images from a spectroscopic imaging experiment using conventional spiral readout (left top) and variable density spiral readout (right top). The logarithmic profile from the center slice is also plotted for each case under the image. The result verifies the simulations performed, where reduced ringing artifacts are seen using the variable density spiral readout. The two images and plots were scaled to be identical so that ringing effects can be viewed at the same level.

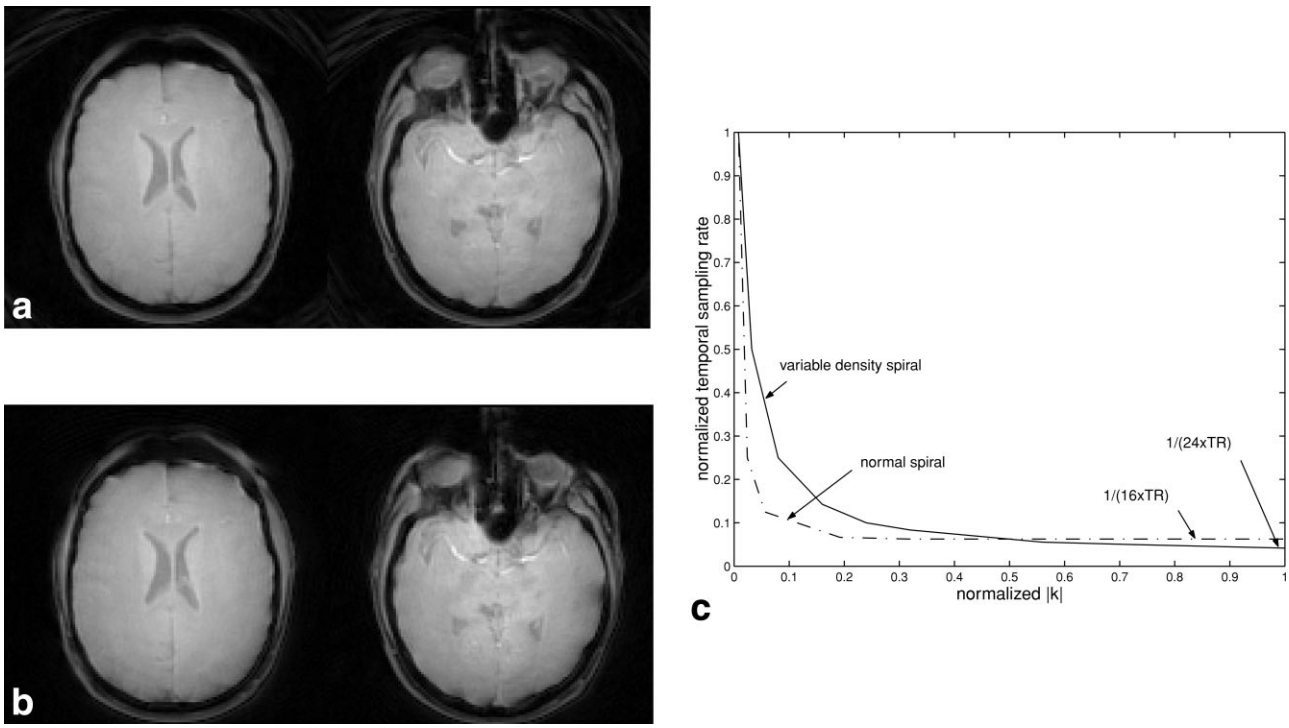

FIG. 5. Comparison of in vivo images obtained using a conventional spiral (**a**) and variable density spiral (**b**) trajectories. 128 × 128 resolution images were obtained over a 20 cm FOV. Sixteen spatial interleaves were used for the conventional spirals, whereas 24 spatial interleaves were used for the variable density spirals in order to keep the readout duration identical in the two acquisitions (4.5 ms). If used in a dynamic imaging mode, (**c**) shows the achievable temporal sampling update rates as a function of *k*-space radius.

frequency component to be sufficiently sampled for reconstruction. Therefore, the update rate is directly related to the density of the sampling trajectory. In this case, we calculated the sampling update rate as the inverse of the distance between successive parts of the trajectory that runs through $k_y = 0$. In the case of variable density spirals, low spatial frequency samples can be updated faster compared to the conventional spirals, while due to the increased number of interleaves, the effective update rate is slower as the trajectory moves further away from the central region. In general, the temporal updating rate of various spatial frequencies can be adjusted by varying the α parameter. Note, an alternative implementation would be to use the same number of interleaves for both variable density and conventional spiral acquisitions at the expense of a longer readout (with a corresponding increase in off-resonance blurring) for the variable density case.

DISCUSSION

An analytic design solution for variable density spirals is given. This design method is implemented in an analogous manner to the work of Glover (9) for conventional spirals. The design approach is also similar to the work by Cline et al. (13) for logarithmic density spirals. Depending on the specific application, the user has control over the following parameters: FOV, resolution, α, matrix size, and the number of spatial interleaves. Since real-time prescription can be done on the scanner, this can potentially be used for real-time imaging where scan parameters are changed on the fly.

In this article, we have illustrated two potential applications using these new trajectory design tools. First, the trajectory design method was used to demonstrate the decreased side lobes in the image point spread function. As pointed out in Ref. 7, the shape of the point-spread function depends on the window used for apodization. Therefore, using various variable density spirals, it is possible to reduce the sidelobes of the point spread function by apodizing with a window which has small side lobes (14). Of note is that in this case, the *k*-space trajectory should cover an extended *k*-space region to maintain resolution and the apodization function should match the applied density to avoid any SNR penalty. The trade off then comes from the extended *k*-space coverage necessary, which will increase the minimum scan time. More spatial/spectral interleaves are used to cover the required *k*-space within the given scan parameters. Nevertheless, for spectroscopic imaging sequences using spiral acquisition, the limiting factor comes from SNR; therefore, an increase in the minimum scan time does not pose a detrimental situation since many averages are normally acquired. A detailed description illustrating the description of variable density spirals in spectroscopic imaging is given in Ref. 7. The feature of improved impulse response has been used in spectroscopic imaging and can further be used for applications where image side lobes can be problematic.

Another example demonstrated was for use in MR fluoroscopy. As shown in Fig. 5, samples from low spatial frequencies can be updated more frequently than conventional spiral acquisitions. This fact naturally extends to other applications as well. Motion-sensitive acquisitions, such as diffusion-weighted imaging, can use the low spatial frequency data to detect and correct gross motion. In this case, navigation can be performed without the need for additional navigator echoes. The oversampling itself also tends to average out any gross motion effects, thereby being more robust in motion-sensitive imaging acquisitions.

Another application that variable density spirals are being used for but not demonstrated in this article is in fast imaging (15). In this case, faster acquisitions are enabled by undersampling the outer *k*-space region, allowing aliasing of the relatively low-energy high spatial frequency information. In the design outlined here, we have critically sampled at the high spatial frequencies. A simple modification to the design algorithm to accommodate this situation can be achieved by changing the number of rotations (n). Originally n was chosen (Eq. [10]) so that it satisfies the Nyquist sampling. A simple relaxation of this can be used for applications where undersampling is desired. For example, if a factor of two undersampling is desired in the outer region of *k*-space, solving for n in Eq. [2] with constraint of:

$$k(1) - k((n-1)/n) = 2/FOV \qquad [13]$$

will give the appropriate value.

The approximation used in Eq. [6] has singular behavior near the origin of *k*-space. This is represented by the increased time it takes the gradients reach its slew-rate limit, as shown in Fig. 2. However, this does not pose any problematic situations whereby the hardware limitations are violated. This approximation and the value of α can be used to control the amount of oversampling near the origin. More oversampling (bigger α) can be desired but at the cost of off-resonance effects, which can be compromised by more spatial interleaving to shorten the trajectory. Analytic expressions which overshoot the approximations in the central region can also be used (see eq. 10 in Ref. 13) near the central *k*-space to shorten this time. Nevertheless, this characteristic of oversampling is a degree of freedom that the user can use for the intended application.

CONCLUSION

A simple analytic solution for variable density spirals is presented. The solution uses a gradient design method which is either slew-rate limited or amplitude limited. The ability to easily calculate variable density spiral waveforms allows flexible implementation on a clinical scanner as well as providing the capability of performing real-time imaging where parameters are altered during the acquisition.

REFERENCES

1. Spielman DM, Pauly JM, Meyer CH. Magnetic resonance fluoroscopy using spirals with variable sampling densities. Magn Reson Med 1995; 34:388–394.
2. Liao JR, Pauly JM, Brosnan TJ, Pelc NJ. Reduction of motion artifacts in cine MRI using variable-density spiral trajectories. Magn Reson Med 1997;37:569–575.
3. Sussman MS, Stainsby JA, Robert N, Wright GA. Variable-density adaptive imaging for high-resolution coronary artery MRI. In: Proc 10th Scientific Meeting ISMRM, Honolulu, 2002. p 374.
4. Tsai CM, Nishimura DG. Reduced aliasing artifacts using variable-density *k*-space sampling trajectories. Magn Reson Med 2000;43:452–458.
5. Lee JH, Nishimura DG. Fast imaging using variable-density spiral trajectories with multi-coil receivers. In: Proc 10th Scientific Meeting ISMRM, Honolulu, 2002. p 2397.
6. Marcei TH, Brooker HR. High-resolution magnetic resonance spectra from a selective region defined with pulsed field gradients. J Magn Reson 1984;57:157–163.
7. Adalsteinsson E, Star-lack J, Meyer CH, Spielman DM. Reduced spatial side lobes in chemical-shift imaging. Magn Reson Med 1999;42:314–323.
8. Meyer CH, Pauly JM, Macovski A. A rapid, graphical method for optimal spiral gradient design. In: Proc 4th Scientific Meeting ISMRM, New York, 1996. p 392.
9. Glover GH. Simple analytic spiral *k*-space algorithm. Magn Reson Med 1999;42:412–415.
10. Hardy CJ, Cline HE. Broadband nuclear magnetic resonance pulses with two-dimensional spatial selectivity. J Appl Phys 1989;66:1513–1516.
11. Kim DH, Adalsteinsson E, Spielman D. PRESS CSI with spiral readout gradients. In: Proc 10th Scientific Meeting ISMRM, Honolulu, 2002. p 2493.
12. Glover GH, Lai S. Self-navigated spiral fMRI: interleaved versus single-shot. Magn Reson Med 1998;39:361–368.
13. Cline HE, Zong X, Gai N. Design of a logarithmic *k*-space spiral trajectory. Magn Reson Med 2001;46:1130–1135.
14. Adalsteinsson E, Spielman D. Filter functions for variable-density spiral CSI. In: Proc 10th Scientific Meeting ISMRM, Honolulu, 2002. p 533.
15. Lee JH, Hargreaves B, Nishimura DG. Fast 3D imaging using variable-density spiral trajectories. In: Proc 9th Scientific Meeting ISMRM, Glasgow, 2001. p 1777.